Journal of Power Sources 270 (2014) 106–112

Contents lists available at ScienceDirect

Journal of Power Sources

journal homepage: www.elsevier.com/locate/jpowsour

High energy density supercapacitors from lignin derived submicron activated carbon fibers in aqueous electrolytes

Sixiao Hu [a], Sanliang Zhang [b], Ning Pan [b, **], You-Lo Hsieh [a, *]

[a] Fiber and Polymer Science, University of California-Davis, One Shields Avenue, Davis, CA 95616, United States
[b] Department of Biological and Agricultural Engineering, University of California-Davis, One Shields Avenue, Davis, CA 95616, United States

HIGHLIGHTS

- Super-fine highly porous activated carbon fibers (ACFs) were derived from lignin.
- Lignin-derived ACFs were fabricated into supercapacitor via vacuum filtration.
- ACFs achieved excellent 344F g^{-1} specific capacitance and 8.1 Wh kg^{-1} energy density.
- KOH ACFs exhibited exceptional total capacitance of 1 F at 10 mg loading.
- Lignin-derived ACFs exhibited over 96% capacitance stability after 5000 cycles.

GRAPHICAL ABSTRACT

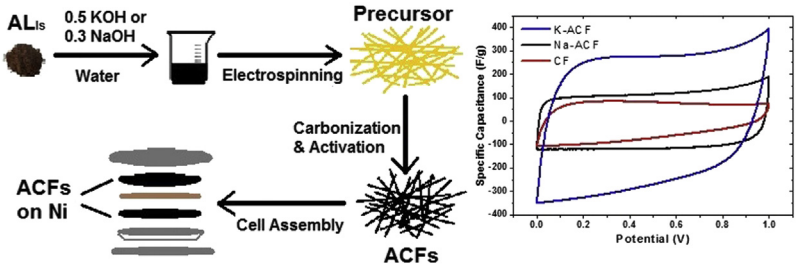

ARTICLE INFO

Article history:
Received 10 March 2014
Received in revised form
1 July 2014
Accepted 10 July 2014
Available online 21 July 2014

Keywords:
Activated carbon fiber
Energy storage
Lignin
Supercapacitor

ABSTRACT

Highly porous submicron activated carbon fibers (ACFs) were robustly generated from low sulfonated alkali lignin and fabricated into supercapacitors for capacitive energy storage. The hydrophilic and high specific surface ACFs exhibited large-size nanographites and good electrical conductivity to demonstrate outstanding electrochemical performance. ACFs from KOH activation, in particular, showed very high 344 F g^{-1} specific capacitance at low 1.8 mg cm^{-2} mass loading and 10 mV s^{-1} scan rate in aqueous electrolytes. Even at relatively high scan rate of 50 mV s^{-1} and mass loading of 10 mg cm^{-2}, a decent specific capacitance of 196 F g^{-1} and a remarkable areal capacitance of 0.55 F cm^{-2} was obtained, leading to high energy density of 8.1 Wh kg^{-1} based on averaged electrodes mass. Furthermore, over 96% capacitance retention rates were achieved after 5000 charge/discharge cycles. Such excellent performance demonstrated great potential of lignin derived carbons for electrical energy storage.

1. Introduction

Activated carbon fibers (ACFs) are highly porous carbon in the fibrous form usually produced via activation of carbon fibers (CFs). The fibrous form of ACFs makes them easy to handle and to be further processed into various forms of sheets, felts and composites. The high specific surfaces, short diffusive paths and abundant accessible pores to sorbates are desirable characteristics of ACFs for removing toxic gases such as SO_2 [1], NO_x [2], organic compounds from air [3] and in waste water [4] as well as in storing hydrogen [5], methane and ethane [6]. Besides those excellent attributes, the high electrical conductivity of ACFs make them good candidate for supercapacitors, a pulse energy storage and delivery device used in the pitch system of wind turbines [7], electric vehicles [8] and

* Corresponding author.
** Corresponding author.
E-mail addresses: npan@ucdavis.edu (N. Pan), ylhsieh@ucdavis.edu (Y.-L. Hsieh).

http://dx.doi.org/10.1016/j.jpowsour.2014.07.063
0378-7753/

actuators [9] to physically uptake and release charges accumulated at the interface of carbon material and the electrolyte. To date, ACF based supercapacitors have been made from phenolic resin fibers in organic electrolytes [10,11] as well as polyacrylnitrile fabrics [12] and polyamic acid electrospun fibers [13] in aqueous electrolytes, yielding a specific capacitance from 113 to 208 F g^{-1}. However, these SCF precursors are energy consuming and expensive to produce and non-renewable. Moreover, the micro porous and carbon structures of those ACFs are not targeted for storing aqueous electrolyte ions. In fact, the electrolyte ions storage capacity of carbons critically depends on the amount of accessible surface area, and such accessibility is largely determined by the micro porous structure and composition, size, defects of the nanographite and the amorphous sp^2 carbon. Overall, high microporosity and wettability [14,15], larger nanographite size and less distorted bond angle [16] favor the adsorption of electrolyte ions. Therefore, it is desirable to fabricate ACFs with controlled micro porous and carbon structures for supercapacitor applications via simple and efficient processes from greener sources.

Lignin is the over 50 million metric tons per year worldwide chemical pulping and biofuel production by-product [17]. With only a small fraction being burned as low-valued fuel [18], lignin represents a significantly under-utilized biomass. The high carbon content and extensively crosslinked polypropanoid structure make lignin an excellent precursor for various carbon materials [19]. Activated carbon particulates have been produced by activation of kraft lignin using alkali hydroxide [20,21], zinc chloride and phosphoric acid [21]. Carbon fibers have been melt spun from softwood and hardwood kraft lignin aided by polyethylene oxide (PEO) [22] and polyethylene terephthalate [23], respectively, and coaxially electrospun from alcell lignin in ethanol [24]. Activated carbon fibers (ACFs) could also be melt spun from acetic acid softwood lignin then steam activation [25] or electrospun from Alcell lignin in ethanol then activated by oxygen-containing species [26]. Recently, we have also electrospun submicron fibers from aqueous alkali lignin with low sulfonate content (AL_{ls}) in-situ impregnated with alkali hydroxide and then simultaneously thermal processed and activated into ACFS in a single-step process [27]. The AL_{ls} based ACFs have very high specific surface (up to 1400 m^2 g^{-1}) with over 85% attributed to micropores at *ca.* 0.7 nm average pore size and remaining mesopores. Such abundant micropores are considered ideal for adsorption of aqueous KOH electrolytes and the mesopores are beneficial to electrolyte transfer to the micropore regions [15], both characteristics being highly promising for applications as supercapacitors.

In this work, AL_{ls} based ACFs were prepared from both NaOH and KOH activation (Na-ACF and K-ACF) and constructed into electrodes and supercapacitors. The electrical conductivities, wettability and microstructures of the ACF electrodes were first evaluated. The electrochemical properties of the ACF supercapacitor cells were thoroughly examined in terms of their specific capacitance from both cyclic voltammetry (CV) and galvanostatic charge/discharge curves, equivalent series resistance (ESR), energy and power densities, as well as cycling stability.

2. Experimental

2.1. Materials

Poly(ethylene oxide) (PEO) (Mw ~600 kDa) and alkali lignin with low sulfonate content (AL_{ls}, Mw ~ 60 kDa, spruce origin) were purchased from Sigma–Aldrich (USA), and sodium hydroxide (anhydrous pellets, A.C.S. grade, 85% minimum purity) and potassium hydroxide (anhydrous pellets, A.C.S. grade 97% minimum purity) were acquired from Fisher Scientific (USA). Nickel foam (≥95% porosity with 80–100 PPI and 1.6 mm in thickness) and button cell case (CR2032) were purchased from MTI Corp (USA). All the materials were used as received.

2.2. Synthesis of activated lignin carbon fibers

Activated carbon fibers were prepared according to a previously reported method [27]. Briefly, aqueous 9/1 w/w AL_{ls}/PEO (10 wt% total concentration) mixtures and without or with alkaline hydroxides at 0.3 NaOH/lignin and 0.5 KOH/lignin were electrospun into CF, Na-ACF and K-ACF precursors, respectively. The electrospun precursor fiber mats were rolled and placed in a quartz tube (2 cm inner diameter) of an electric furnace (Mini-Mite, Lindberg/Blue). Carbonization (and simultaneous activation for ACFs) was performed by first heating to 105 °C to drive off the moisture, then heating to 850 °C, both at 10 °C min^{-1} heating rate and held at each temperature for 0.5 h under flowing N_2 at 100 mL min^{-1}. The heat processed fibers were cooled to ambient temperature within 12 h, under flowing N_2 at 100 mL min^{-1}. CFs and both ACFs were then washed with deionized water to remove residual alkali metals and other small hydrocarbon impurities, followed by oven drying at 105 °C for 0.5 h.

2.3. Construction of electrode and supercapacitor cell

The CF and ACF mats were dispersed in water (1 g L^{-1}) and sonicated (2510, Branson) for 30 min. The electrodes were prepared by vacuum filtration [28] of either CF or ACF suspensions to deposit onto nickel foams (shown in Scheme 1a). The weight of nickel foam per electrode is *ca.* 60 mg. The loaded mass of CF and Na-ACF was weighed to be 5.4 and 3.2 mg, respectively and the mass of K-ACFs varied from 1.8, 3.5, 7.5 to 10.0 mg and denoted as K-ACF-1, 2, 3 to 4. The resulting electrodes were roller pressed to 0.1–0.2 mm thickness and mold punched into 1.5 cm diameter circular shaped cells. The supercapacitor cells were constructed by using two identical electrodes with cellulose filter paper as separator into symmetric button cells (Scheme 1b) and sealed with a manual crimper (CR2032, MTI). 6 M aqueous KOH was the electrolytes.

2.4. Analytical methods

The chemical structures of CF and ACFs were examined by Fourier transform infrared spectroscopy (FTIR) (Nicolet 6700, Thermo Scientific). All FTIR spectra were collected using samples

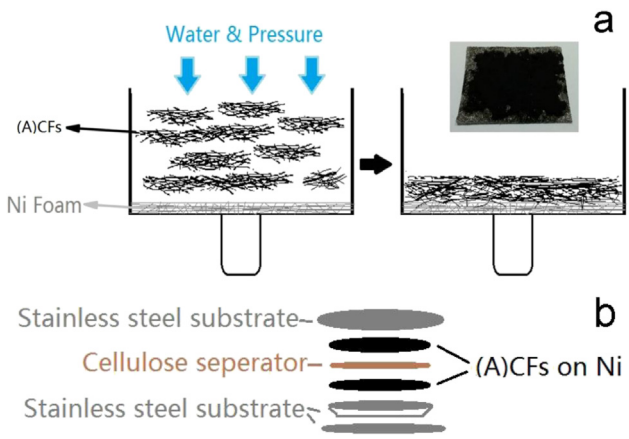

Scheme 1. Construction of (a) an electrode by CF and ACF deposition onto nickel foam via vacuum filtration (inset image: photo of an electrode); (b) a symmetric supercapacitor button cell.

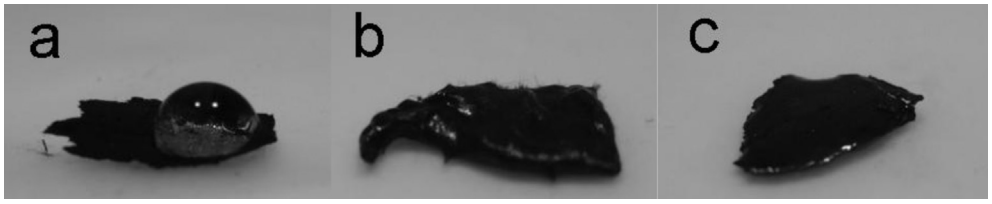

Fig. 1. Wetting of (a) CF; (b) Na-ACF and (c) K-ACF.

dried at 60 °C for 12 h and pressed with anhydrous KBr powders into pellets. The sp^2 and sp^3 carbon configuration and proportion of CF and ACFs were investigated by Raman spectroscopy (RM1000, Renishaw) with excitation source of a 514.5 nm Ar line, and their electric resistivities measured by a four-point probe (HM21, Jandel). Five measurements were taken at different spots of each sample and the averaged peak of these 5 trials was used for the Raman analysis.

The electrochemical properties of the supercapacitors were analyzed by CV tests on a potentiostat/galvanostat (263A, EG&G Princeton Applied Research) and electrochemical impedance spectroscopy (EIS) with a frequency response detector (263A, EG&G) over 10 mHz to 100 kHz frequencies at room temperature. The gravimetric specific capacitance from the CV curve (C_{c-v}) and galvanostatic charge/discharge curve were derived (C_{i-t}) via Eqs. (1) and (2), respectively. The areal capacitance (C_a) normalized by the area of single electrode was calculated via Eq. (3). The ESR (R_{ESR}) from charge/discharge curve was derived via Eq. (4), and the energy and power densities of single electrode were calculated from Eqs. (5) and (6), respectively. V is the operating voltage, ΔV the voltage change (1 V), I_m the discharge current normalized by the mass of single electrode, Δt the discharge time, A the area of single electrode, m the mass of single electrode, $\Delta V_{initial}$ the initial potential drop from the galvanostatic discharge curve.

$$C_{c-v} = \frac{\int_0^V C\,dV}{\Delta V} \quad (1)$$

$$C_{i-t} = \frac{2 \times I_m \times dt}{dV} \quad (2)$$

$$C_a = \frac{C_{c-v} \times m}{2A} \quad (3)$$

$$R_{ESR} = \frac{\Delta V_{initial}}{I_m} \quad (4)$$

$$E = \frac{C_{c-v} \times V^2}{8} \quad (5)$$

$$P = \frac{V^2}{4 \times R_{ESR} \times \overline{m}} \quad (6)$$

3. Results and discussion

3.1. Wettability, chemical and carbon structures of CF and ACF electrodes

Owning to their continuous fiber form, CFs and ACFs could be deposited onto nickel foam from their aqueous suspension via simple vacuum filtration [28] without needing any adhesives (Scheme 1). In water, CF samples stayed floated on top while ACFs remain thoroughly dispersed, displaying their distinctly different water wetting behaviors. Water droplets place on these fibrous mats further confirm their different wetting behaviors, i.e., hydrophobic CFs shown by the slightly larger than 90° water contact angle (Fig. 1a) hydrophilic ACFs by the immediate spreading of water droplets (Fig. 1b and c). The FTIR spectrum (Fig. 2) of CF and both ACFs showed the same characteristic skeletal C=C stretching of aromatic hydrocarbons at 1567 cm^{-1}, 3438 and 1630 cm^{-1} peaks ascribing to OH stretching and bending, respectively, as well as the C–O stretching at 1113 cm^{-1}. The slightly more intense OH bending and C–O stretching peaks of ACFs, indicating ACFs to be more hydrophilic than CFs, consistent with their better water wetting behavior. Despite of their similarly high carbon contents of *ca.* 94 wt% [27], the more hydrophilic ACFs are attributed to their greater extents of polar groups generated from alkali hydroxide activation (see Fig. 3).

The Raman spectrum of CF and ACFs showed rather broad and prominent G and D peaks in the 1500 to 1600 and 1300 to 1400 cm^{-1} ranges, respectively. The G and D peaks were further resolved into G1 & D1 and G2 & D2 peaks to represent the winding short basal plane with bond angle order and amorphous sp^2 carbon clusters with bond disorder, respectively, following same deconvolution technique for various non-graphitic carbons [29–31]. The basal planes likely indicated the existence of nanocrystalline graphite consisting of lignin benzene rings and conjugated aromatic hydrocarbons from carbonization while the sp^2 carbon clusters could be from the non-aromatic hydrocarbons. Such classification is consistent with the three stage graphene to diamond amorphization model, in which the peaks in 1580–1600 cm^{-1} and 1530 to 1560 cm^{-1} ranges represent the nanocrystalline G peak and amorphous sp^2 carbon clusters, respectively [32].

The full width at high maximum (FWHM) of G1and D2 peaks increased from 66 cm^{-1} in CF to 75 cm^{-1} in both ACFs, indicating

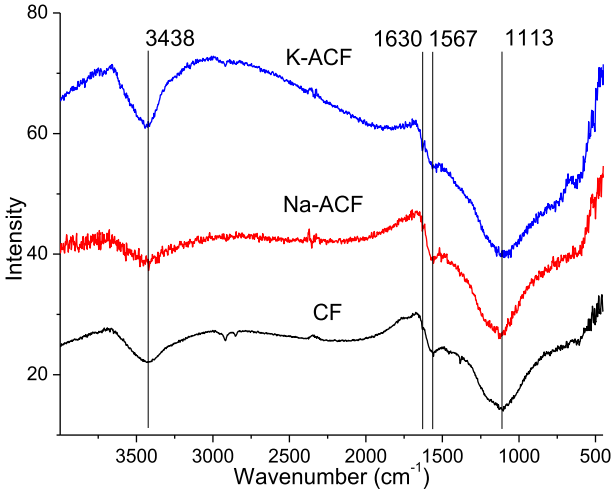

Fig. 2. FTIR spectrum of (a) CF; (b) Na-ACF and (c) K-ACF.

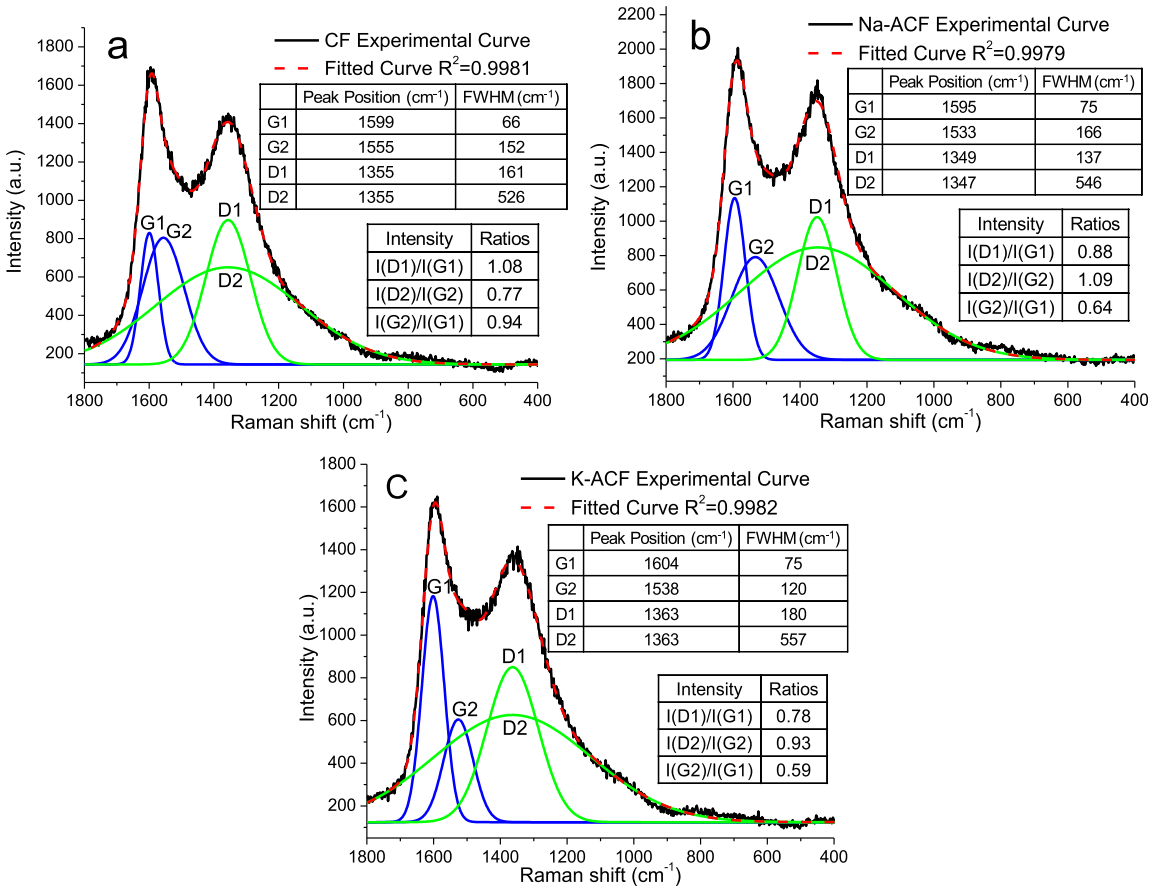

Fig. 3. Raman spectra of (a) CF; (b) Na-ACF and (c) K-ACF.

increased bond disorder of the basal planes from activation. This is also consistent with the increased electric resistance from *ca.* 6 Ω cm^{-1} for CF to 10 Ω cm^{-1} for ACFs. The FWHM of D2 peak slightly increased from 526 cm^{-1} in CF to 546 cm^{-1} in Na-ACF and to 557 cm^{-1} in K-ACF, also suggesting more defective species in the amorphous sp^2 carbon clusters from activation. Noted such changes in the deconvoluted D2 peaks FWHM could be less accurate due to the fitting methods itself, since the D peaks could be the lower frequency shoulder of the G peaks [32]. The I(D1)/I(G1) ratio decreased from 1.08 in CF to 0.88 in Na-ACF and 0.78 in K-ACF. As I(D)/I(G) ratio is reciprocal to nanographite size but proportional to amorphous sp^2 carbon size [32], the lowered I(D)/I(G) ratios of ACFs indicated increased basal plane sizes. The increased I(D2)/I(G2) ratio from 0.77 in CF to 1.09 in Na-ACF and 0.93 in K-ACF also suggest increased amorphous sp^2 carbon cluster sizes from activation. The I(G2)/I(G1) ratio, an empirical parameter indicative the relative disordered to ordered contents [29], decreased from 0.94 in CF to 0.64 in Na-ACF and 0.59 in K-ACF. As potassium had lower ionization energy than sodium, the reaction between KOH and carbon was more violent, producing more defective sp^2 carbon clusters in K-ACF, e.g. higher FWHM of D2 peak, as well as a higher content of ordered species, e.g. lowest I(G2)/I(G1) ratio. These changes in Raman spectrum showed that oxidative activation of the lignin carbon chars by alkali hydroxide produced more reactive but less disordered amorphous sp^2 carbons. In other words, oxidative activation consumes the disordered amorphous sp^2 carbon to increase the proportion of the more ordered domains and produces polar groups to increase hydrophilicity of ACFs.

3.2. Electrochemical performance of supercapacitors

The electrochemical properties of symmetric supercapacitors assembled from CF and ACF were studied. The CV curve (Fig. 4a, red line in the web version) of the CF cells was irregular and covered a relatively small area, indicating small capacitance. The two ACF cells, on the other hand, showed rather rectangular CV curves (Fig. 4a, black and blue lines in the web version), typical of double layer capacitors. At the scan rate of 50 mV s^{-1}, the CF cell exhibited specific capacitance of 66 F g^{-1}, while Na-ACF and K-ACF-1 cells showed doubled and quadrupled capacitance of 122 and 267 F g^{-1}, respectively. The significantly increased capacitance for these ACF cells was attributed mainly to their much larger specific surface area and improved hydrophilicity. K-ACF outperformed Na-ACF by more than double the specific capacitance. Although both ACFs had similar specific surface area, the micropores in K-ACF were mostly around 0.75 nm in sizes, whereas those in Na-ACF were more widely distributed between 0.8 and 1.2 nm. [27] Such differences in pore sizes ad pore size distribution could be the determining factor of the more superior specific capacitance of the K-ACF than Na-ACF. Another possible contributing factor could be the larger graphite basal plane sizes in K-ACF, beneficial for the charge storage as indicated by the preceding Raman analysis [16].

Moreover, K-ACF also showed the highest areal capacitance, which increased with the mass of electrodes (Fig. 4b). At 50 mV s^{-1} scan rate and 10 mg electrode mass, a relatively high areal capacitance of 0.55 F cm^{-2} was achieved, giving rise to a remarkable total capacitance of 1 F per electrode [33]. The specific capacitance of K-ACFs at 50 mV s^{-1} scan rate decreased from 267 to 196 F g^{-1} when

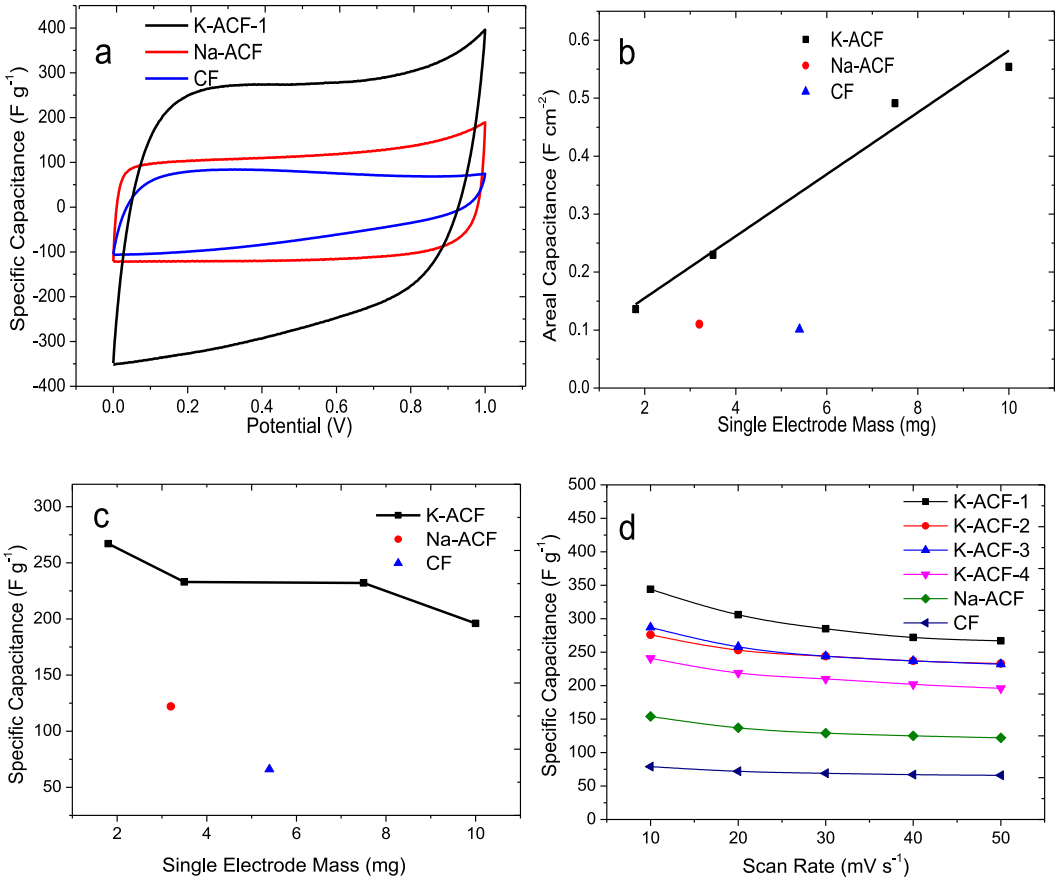

Fig. 4. (a) Cyclic voltammogram; (b) the areal capacitance and (c) specific capacitance as a function of electrode mass at scan rate of 50 mV s^{-1}; (d) specific capacitance as a function of scan rate.

the electrode mass increased from 1.8 to 10 mg (Fig. 4c). This could be due to the thicker and more tightly packed electrode that lowers the electrolyte diffusion rate [34,35], noting that the roller pressing process packs an electrode with high mass to suite to the fixed electrode thickness. The specific capacitances of all cells were found to decrease with increasing scan rate (Fig. 4d), caused by shorter ion migration time at faster rate [36]. For K-ACFs, an outstanding specific capacitance of 344 F g^{-1} was obtained at electrode mass of 1.8 mg and scan rate of 10 mV s^{-1}, validating that ACFs, K-ACF in particular, exhibited excellent electrochemical properties. The produced specific capacitances are much higher than that of unactivated lignin based sub-micron carbon fiber (67 F g^{-1}) [37] and lignin-based mesoporous carbon (102.3 F g^{-1}) [38]. Moreover, at a relatively high scanning of 50 mV s^{-1}, 4.3 and 8.1 Wh kg^{-1} energy densities were achieved for Na-ACF and K-ACF respectively, showing either comparable (Na-ACF) to, or much better performance (K-ACF) than the 3–5 Wh kg^{-1} energy density of commercialized activated carbon [9].

Deriving from the galvanostatic charge/discharge curve at 1 A g^{-1}, the specific capacitances of K-ACF-1 and Na-ACF were 316

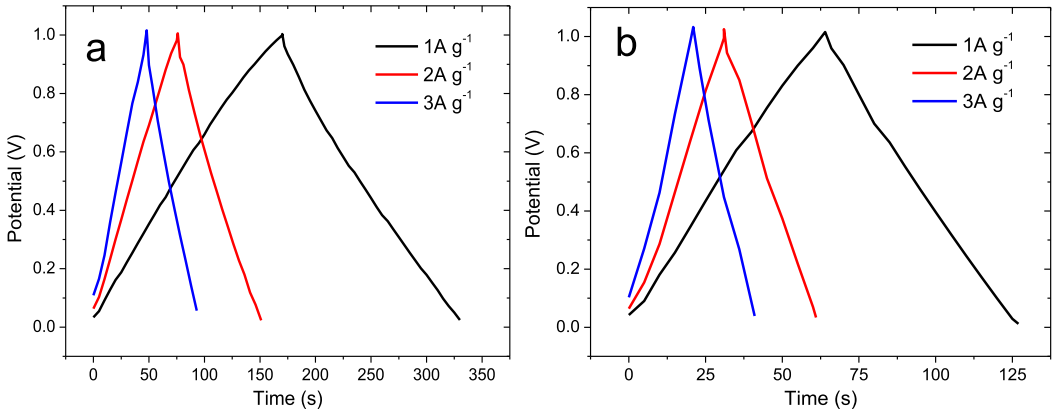

Fig. 5. Galvanostatic charge/discharge curves of (a) K-ACF-1 and (b) Na-ACF at various current densities.

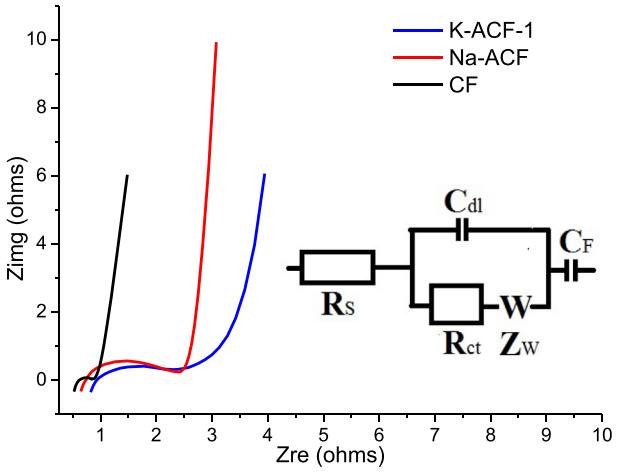

Fig. 6. Nyquist plots of K-ACF-1, Na-ACF and CF scanned from 100 mHz to 100 kHz.

and 122 F g^{-1}, respectively, agreeing well with the values derived from the CV curves. The IR drop, which is the initial onset point of the charging curve, increased from 41.9 to 81.3 then to 119.1 mV for K-ACF-1, and from 55.2 to 81.5 then to 140.4 mV for Na-ACF, respectively, when the current density rose from 1 to 2 then to 3 A g^{-1} (Fig. 5). The relatively linear increase in the voltage with increasing current density suggested the ESRs of both ACFs remained approximately constant. This indicated the high current density had little effects on ACF surface, porous and carbon structures. The ESR*s* of both K-ACF-1 and Na-ACF at 1 A g^{-1} were estimated following Eq. (4) to be 23.3 and 17.3 Ω, respectively. The smaller resistance of Na-ACF was also consistent with the more rectangular shape of its CV curve (Fig. 4a). Based on these ESR*s* from the discharge curves, the power densities for K-ACF-1 and Na-ACF cells at 1 A g^{-1} were calculated using Eq. (5) as 2.98 and 2.26 kW kg^{-1}, respectively. It should be noted that, unlike many previous publications [28,39,40], the ESR values from the charge/discharge curves were used, not those from the Nyquist plot which gives much smaller ESR values and consequently a higher power density. From the Nyquist plots scanned from 100 kHz to 10 mHz (Fig. 6), much smaller ESR values of 1.71, 1.43 and 0.81 Ω were derived for K-ACF-1, Na-ACF and CF, respectively. A modified Randles model was used as the equivalent circuit where R_s represents the ionic resistance of electrolytes, R_{ct} is the charge-transfer resistance from electrolytes moving through the electrodes during kinetically-controlled electrochemical reactions, Z_w is the Warburg impedance associated with 1-D linear semi-infinite diffusion of electrolytes to/from the flat electrode planes, C_{dl} is the double layer capacitance and C_f is the faradic capacitance [41,42] The Nyquist plot showed a larger semi-circle in ACFs than in CF. Although the R_s of all CF and ACFs were similarly located in a narrow range of 0.5–0.8 Ω, the R_{ct} of ACF is much larger than that of CFs, which may result from the formation of more reactive groups in ACFs after activations. The knee frequencies of ACFs are also considerably lower than that of CF, suggesting decreased ion diffusion ability to the carbon planes possibly when electrolytes were diffused into small micropores in the bulk ACFs that are comparable to them in sizes. All these observations suggested increased resistivity in ACFs than CF, consistent with the surface resistivity test (see Fig. 7).

In addition, the stability of the as-prepared ACF cells was examined over 5000 charge/discharge cycles at constant current densities to show 96.5 and 96.1% retention of capacitance for K-ACF and Na-ACF cells, respectively. Their high cycling stability is comparable to graphene based electrodes [28].

4. Conclusion

CF, NaOH and KOH activated ACFs were efficiently prepared from AL_{ls} and the ACFs were fabricated into supercapacitors. Activation via alkaline hydroxides turned the rather hydrophobic CFs into hydrophilic and readily water wettable ACFs that had different carbonaceous structures than CF, i.e., larger basal plane sizes and more defective sp^2 amorphous carbon, attributing to the excellent electrochemical properties of the ACF supercapacitors. The K-ACF supercapacitor, in particular, achieved a remarkable 344 F g^{-1} specific capacitance at a low electrode mass of 1.8 mg and 10 mV s^{-1} scan rate and maintained at 196 F g^{-1} at an even higher 10 mg mass and 50 mV s^{-1} rate, giving rise to a high average energy density of 8.1 Wh kg^{-1} at 50 mV s^{-1} scan rate. The superior electrochemical properties of supercapacitor constructed with K-ACF over Na-ACF were attributed mainly to the higher microporosity and more narrowly distributed *ca.* 0.75 nm pore size, possibly due to the larger basal plane of the nanographites. The constructed supercapacitor cells from both ACFs showed rather low ESR and outstanding cycling stability, affirming AL_{ls} based ACFs to be excellent carbonaceous electrodes for supercapacitors in aqueous electrolytes. This demonstrates the outstanding potential for converting the abundant lignocellulosic biomass into high performance carbon materials for energy storage.

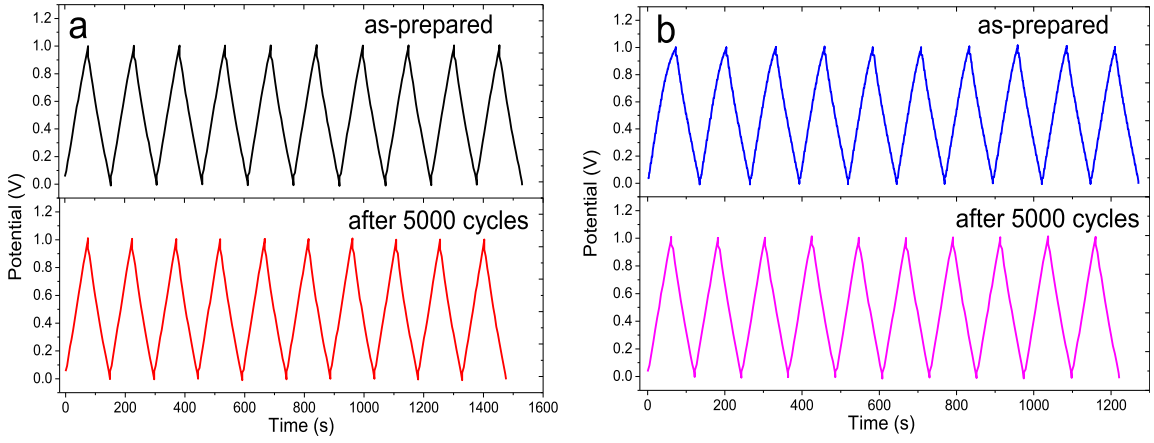

Fig. 7. Cell performance comparison of (a) K-ACF-1 and (b) Na-ACF cells as-prepared and after 5000 cycles' charge/discharge.

Acknowledgments

The support for this work from California EISG 12-02TE Grant is greatly appreciated.

References

[1] M.A. Daley, C.L. Mangun, J.A. DeBarr, S. Riha, A.A. Lizzio, G.L. Donnals, J. Economy, Carbon 35 (1997) 411–417.
[2] I. Mochida, S. Kawano, M. Hironaka, S. Yatsunami, Y. Korai, Y. Matsumura, M. Yoshikawa, Chem. Lett. (1995) 385–386.
[3] M. Lordgooei, K.R. Carmichael, T.W. Kelly, M.J. Rood, S.M. Larson, Gas Sep. Purif. 10 (1996) 123–130.
[4] S.H. Lin, F.M. Hsu, Ind. Eng. Chem. Res. 34 (1995) 2110–2116.
[5] M.A. de la Casa-Lillo, F. Lamari-Darkrim, D. Cazorla-Amoros, A. Linares-Solano, J. Phys. Chem. B 106 (2002) 10930–10934.
[6] S.Y. Jiang, J.A. Zollweg, K.E. Gubbins, J. Phys. Chem. 98 (1994) 5709–5713.
[7] C. Abbey, G. Joos, IEEE Trans. Ind. Appl. 43 (2007) 769–776.
[8] P. Ball, Y. Gogotsi, MRS Bull. 37 (2012) 802–803.
[9] A. Burke, M. Miller, J. Power Sources 196 (2011) 514–522.
[10] I. Tanahashi, A. Yoshida, A. Nishino, Carbon 28 (1990) 477–482.
[11] I. Tanahashi, A. Yoshida, A. Nishino, Carbon 29 (1991) 1033–1037.
[12] B. Xu, F. Wu, S. Chen, C. Zhang, G. Cao, Y. Yang, Electrochim. Acta 52 (2007) 4595–4598.
[13] C. Kim, Y.-O. Choi, W.-J. Lee, K.-S. Yang, Electrochim. Acta 50 (2004) 883–887.
[14] A. Ghosh, Y.H. Lee, ChemSusChem 5 (2012) 480–499.
[15] G. Gryglewicz, J. Machnikowski, E. Lorenc-Grabowska, G. Lota, E. Frackowiak, Electrochim. Acta 50 (2005) 1197–1206.
[16] R.S. Ruoff, in: MRS Spring Meeting, San Francisco, CA, 2013.
[17] C.S.A. Higson, in: 2011.
[18] J. Zakzeski, P.C.A. Bruijnincx, A.L. Jongerius, B.M. Weckhuysen, Chem. Rev. 110 (2010) 3552–3599.
[19] I.A. Pearl, The Chemistry of Lignin, in: Irwin A. Pearl (Ed.), Dekker, 1967, pp. 106–127.
[20] V. Fierro, V. Torne-Fernandez, A. Celzard, Microporous Mesoporous Mater. 101 (2007) 419–431.
[21] J. Hayashi, A. Kazehaya, K. Muroyama, A.P. Watkinson, Carbon 38 (2000) 1873–1878.
[22] J.F. Kadla, S. Kubo, R.A. Venditti, R.D. Gilbert, A.L. Compere, W. Griffith, Carbon 40 (2002) 2913–2920.
[23] S. Kubo, J.F. Kadla, J. Polym. Environ. 13 (2005) 97–105.
[24] M. Lallave, J. Bedia, R. Ruiz-Rosas, J. Rodriguez-Mirasol, T. Cordero, J.C. Otero, M. Marquez, A. Barrero, I.G. Loscertales, Adv. Mater. 19 (2007) 4292–4296.
[25] Y. Uraki, A. Nakatani, S. Kubo, Y. Sano, J. Wood Sci. 47 (2001) 465–469.
[26] R. Ruiz-Rosas, J. Bedia, M. Lallave, I.G. Loscertales, A. Barrero, J. Rodriguez-Mirasol, T. Cordero, Carbon 48 (2010) 696–705.
[27] S. Hu, Y.L. Hsieh, J. Mater. Chem. A 1 (2013) 11279–11288.
[28] S. Zhang, Y. Li, N. Pan, J. Power Sources 206 (2012) 476–482.
[29] N. Shimodaira, A. Masui, J. Appl. Phys. 92 (2002) 902–909.
[30] M. Schmirler, F. Glenk, B.J.M. Etzold, Carbon 49 (2011) 3679–3686.
[31] J.S. Macedo, L. Otubo, O.P. Ferreira, L.D.F. Gimenez, I.O. Mazali, L.S. Barreto, Microporous Mesoporous Mater. 107 (2008) 276–285.
[32] A.C. Ferrari, J. Robertson, Phys. Rev. B 61 (2000) 14095–14107.
[33] D. Zhang, Y. Sun, L. Chen, S. Zhang, N. Pan, Mater. Des. 54 (2014) 315–322.
[34] M.D. Stoller, R.S. Ruoff, Energy Environ. Sci. 3 (2010) 1294.
[35] Y. Gogotsi, P. Simon, Science 334 (2011) 917–918.
[36] S. Zhang, N. Pan, J. Mater. Chem. A 1 (2013) 7957–7962.
[37] C. Lai, Z. Zhou, L. Zhang, X. Wang, Q. Zhou, Y. Zhao, Y. Wang, X.-F. Wu, Z. Zhu, H. Fong, J. Power Sources 247 (2014) 134–141.
[38] D. Saha, Y. Li, Z. Bi, J. Chen, J.K. Keum, D.K. Hensley, H.A. Grappe, H.M. Meyer 3rd, S. Dai, M.P. Paranthaman, A.K. Naskar, Langmuir 30 (3) (2014) 900–910.
[39] M. Stoller, S. Park, Y. Zhu, J. An, R. Ruoff, Nano Lett. 8 (2008) 3498–3502.
[40] Y. Jang, J. Jo, Y.-M. Choi, I. Kim, S.-H. Lee, D. Kim, S.M. Yoon, Electrochim. Acta 102 (2013) 240–245.
[41] J.E.B. Randles, Discuss. Faraday Soc. 1 (1947) 11–19.
[42] K.H. Kim, M. Yang, K.M. Cho, Y.S. Jun, S.B. Lee, H.T. Jung, Sci. Rep UK 3 (2013).